Design study for transmission improvement of resonant surface plasmons using dielectric diffraction gratings

Seung Ho Choi,[1] Sung June Kim,[1,2] and Kyung Min Byun[3,*]

[1]Interdisciplinary Program of Bioengineering, Seoul National University, Seoul, South Korea 152-742

[2]School of Electrical Engineering, Seoul National University, Seoul, South Korea 151-742

[3]Department of Biomedical Engineering, Kyung Hee University, Yongin, South Korea 446-701

*Corresponding author: kmbyun@khu.ac.kr

Received 15 December 2008; revised 30 March 2009; accepted 23 April 2009;
posted 28 April 2009 (Doc. ID 105358); published 15 May 2009

A transmission-type surface plasmon resonance configuration with dielectric gratings regularly patterned on a silver film was investigated with the aim of enhancing the diffraction efficiency of radiative surface plasmons. The theoretical work was conducted using rigorous coupled-wave analysis in terms of first order diffraction efficiency and conversion efficiency (CE). The results show that pyramid gratings can produce a higher transmittance compared with other grating profiles. Design optimization of the pyramid grating at a wide range of grating thicknesses and periods resulted in a maximum transmittance that was larger than 77% and a peak CE of about 85%. This study demonstrates the potential of using transmitted surface plasmon waves in various optical devices, such as optical biosensors, optical imaging systems, and polarization filters. © 2009 Optical Society of America

OCIS codes: 050.2770, 240.6680, 310.0310.

1. Introduction

Surface plasmon resonance (SPR) has drawn large interest over the past two decades due to its potential use in various optical devices [1–3]. When a polarized light is incident on a dielectric–metal interface through a glass substrate under total internal reflection, the surface electron density becomes coherent fluctuation on the metal surface, which is accompanied by surface plasmon (SP) waves decaying exponentially into both media [4]. When the momentum of incident beam matches that of the collective charge oscillation, SPR occurs and SP waves are highly excited. This feature of SPs enables to localize and guide the light in subwavelength metallic structures and to construct integrated optoelectronic circuits with subwavelength components, such as waveguides, switches, and modulators, which can be employed to carry optical signals to different parts of the circuit [5]. Moreover, since the resonance condition is sensitive to the permittivity of a dielectric medium surrounding the metal film, SPR technique can be used for surface-limited optical detection, e.g., a microscopic imaging system [6] or a label-free optical biosensor.

A conventional SPR structure based on the Kretschmann configuration has a confined penetration depth, for example, of 100–200 nm for a silver/air interface at $\lambda = 532$ nm [7], and its detection range is intrinsically limited to the plasmon decay length. On the other hand, a transmission-type SPR configuration enables SP waves to radiate into the air space and can allow for the investigation of thick and bulky targets by measuring transmission or scattering characteristics, as well as for the development of an optical apparatus, e.g., an optical modulator or polarization filter. The light emission of a propagating SP has been extensively investigated in Ref. [4]. When the roughness of a metal surface is in the

0003-6935/09/152924-08$15.00/0

range of less than 2 nm, nonradiative plasmons become radiative as a result of SP–photon coupling via roughness. Although it has been shown that the intensity and angular distributions of the emitted light could be controlled by surface roughness, practically it is difficult to adjust random surface parameters and to achieve reproducible results in experiments. Furthermore, for surface roughness higher than 2 nm, it is not possible to outcouple excited plasmons efficiently as the transmitted light is strongly scattered and moves with increased disorder. As a result, most of the earlier studies based on corrugated metal surfaces used the converted radiation modes, which may not have enough intensity to be associated with other external optical systems [8,9].

To overcome this restriction, Park *et al.* proposed using dielectric diffraction gratings for the efficient transformation of SP waves into transmission modes [10]. From this study, a combination of the conventional Kretschmann configuration with rectangular gratings on a silver film yielded a peak outcoupling efficiency of 50%. Figure 1 presents the calculated diffraction efficiency of SP waves at a grating thickness = 50 nm, a period = 600 nm, and a fill factor = 50%. When TM-polarized light at $\lambda =$ 633 nm was incident on a BK7 prism substrate with an incidence angle of 46.55°, resonantly excited SP waves propagated along the metal surface and diffracted light with a transmittance of 17.5% was generated by surface-relief dielectric gratings. However, when the 40 nm thick silver film was eliminated, no plasmon wave was formed, and the evanescent field induced by total internal reflection was diffracted at the prism–grating boundary. It was confirmed from Fig. 1 that the outcoupling associated with SP waves was significantly larger (by more than 40 times) than that of evanescent fields on account of the strong excitations of plasmon fields. Lenaerts *et al.* achieved a diffraction efficiency of 68% using a modified SPR

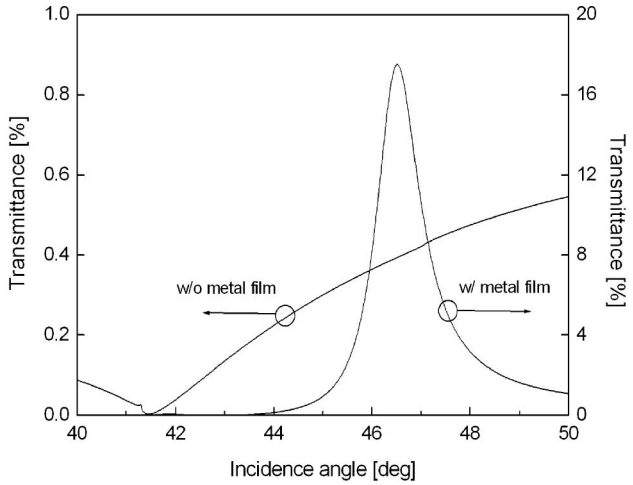

Fig. 1. Transmittance curves of the first-order beams diffracted by dielectric gratings deposited on an attenuated total reflection configuration with and without a metal film. A 40 nm thick silver film with a dielectric function of $-18 + 0.5i$ at $\lambda = 633$ nm was used as the metal layer [10].

structure in which a waveguide grating was employed on a metal surface [11]. We have also recently investigated rectangular gratings for an effective outcoupling of SPs, in addition to examining their practical application as an optical biosensor [12]. Enhanced transmittance of up to 65% and 53% was predicted numerically for a dielectric and metallic grating, respectively.

However, since the diffraction efficiency can be significantly influenced by the grating profile as well [13], in this study, design optimization for an enhanced diffraction efficiency was explored for various grating profiles. To assess the effects of the grating profile on the transmission efficiency and to determine the optimal grating structure for maximum transmittance of SP waves, the transmission efficiency was investigated for a wide range of grating periods and thicknesses. The results of this study hold potential for advancing the use of radiative SP fields in biomolecular sensing, imaging, and other optical devices.

This paper is organized as follows. In Section 2, a numerical model based on the rigorous coupled-wave analysis (RCWA) [14,15] is described. Results of the transmission characteristics for the various design parameters of the dielectric grating are presented in Section 3 with the aim to maximize the diffraction efficiency of propagating SP waves. Concluding remarks are discussed in Section 4.

2. Numerical Model

A schematic diagram of the transmission-type SPR configuration with dielectric gratings is shown in Fig. 2(a). One-dimensional diffraction gratings with a period Λ are regularly patterned on a metal film supporting the SP waves. A 40 nm thick silver layer is deposited on a prism substrate through which a polarized light is incident with a wavelength $\lambda =$ 633 nm. A fill factor (f), which is the ratio of the volume occupied by the gratings, is fixed at $f = 50\%$ to exclude the influence of grating volume on the diffraction efficiency. The optical constants (n, k) of BK7 glass substrate, silver film, and dielectric gratings were determined as (1.515, 0), (0.059, 4.243), and (1.5, 0) [e.g., polymethyl methacrylate (PMMA)], respectively, at $\lambda = 633$ nm [10,16]. Figure 2(b) shows a cross-sectional view of four different grating profiles, which are modeled as a rectangle, pyramid, left-biased sawtooth, and right-biased sawtooth, respectively.

The dispersion relation associated with the resonance conditions of SP waves is given by

$$k_{\mathrm{SPR}} = k_0 \sqrt{\varepsilon_p} \sin \theta_{\mathrm{SPR}}, \tag{1}$$

where k_{SPR} and k_0 $(= w/c)$ are the wave vectors of the SP and the incident light. Also, w is the angular frequency of the incident light, c is the speed of light, and ε_p and θ_{SPR} are the dielectric function of a prism substrate and the incidence angle at resonance. A propagating SP is converted into a radiation mode

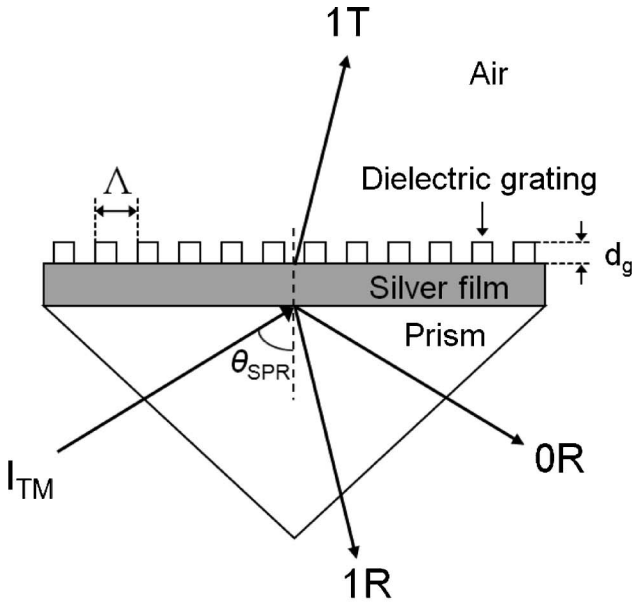

(a)

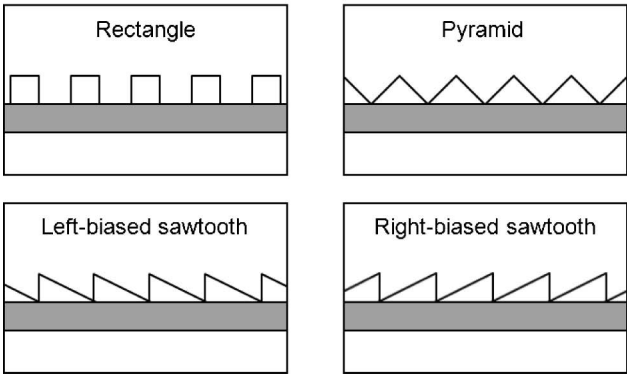

(b)

Fig. 2. (a) Schematic diagram of a transmission-type SPR configuration with dielectric gratings. A thin silver film with a thickness of 40 nm is deposited on a prism substrate. PMMA dielectric gratings with a period Λ and a thickness d_g are regularly patterned on the metal layer. TM-polarized light is incident through the prism substrate at a fixed wavelength of $\lambda = 633$ nm. The transmitted light radiates into the air environment. (b) Rectangle, pyramid, left-biased sawtooth, and right-biased sawtooth dielectric grating profiles. The fill factor is fixed at $f = 0.5$.

by a diffraction grating when momentum matching between SPs and photons is satisfied. This condition is expressed as

$$k_i = k_{\mathrm{SPR}} - iK = k_0\sqrt{\varepsilon_p}\sin\theta_{\mathrm{SPR}} - i\frac{2\pi}{\Lambda},$$
$$i = 0,\ \pm 1,\ \pm 2,\ \ldots, \tag{2}$$

where k_i is the wave vector of the transmitted light with ith diffraction order, K is the grating vector, and Λ is the grating period. The angles of the ith forward and backward diffracted light are given by

$$\theta_i^{\mathrm{T}} = \sin^{-1}\left(\frac{k_i}{k_0}\right), \tag{3}$$

$$\theta_i^{\mathrm{R}} = \sin^{-1}\left(\frac{k_i}{\sqrt{\varepsilon_p}k_0}\right). \tag{4}$$

The number of transmitted beams is determined by the diffraction angle that satisfies the above relations. In this study, a limited range of grating periods (300 nm to 600 nm) is considered, so that only the low diffraction orders can radiate into the air.

For numerical analyses, we employed the RCWA method, which has been successfully used to explain the experimental results of grating structures. Our RCWA routine was found to corroborate the experiments of earlier SPR studies using periodic nanowires [17,18]. Convergence in RCWA calculation was achieved by including 30 space harmonic orders and by discretizing a continuous grating profile into 16 slice layers with an equal thickness.

3. Results and Discussion

For efficient detection of transmitted light and its application to various optical devices, higher transmittance is required. Figure 3 presents the calculated zeroth-order reflection (0R) and the first-order transmission (1T) curves for a SPR structure with rectangular dielectric gratings when the grating thicknesses are $d_g = 30$ nm, 60 nm, 90 nm, 120 nm, 180 nm, 240 nm, and 300 nm. The PMMA grating has a period of $\Lambda = 600$ nm and a width of 300 nm (i.e., $f = 50\%$). Resonance angle obviously increases with the grating thickness, and significant outcoupling of the propagating SPs of more than 30% occurs at $d_g > 60$ nm.

Figure 4 shows that the resonance and transmittance characteristics are strongly dependent on the grating thickness. As shown in Fig. 4(a), the

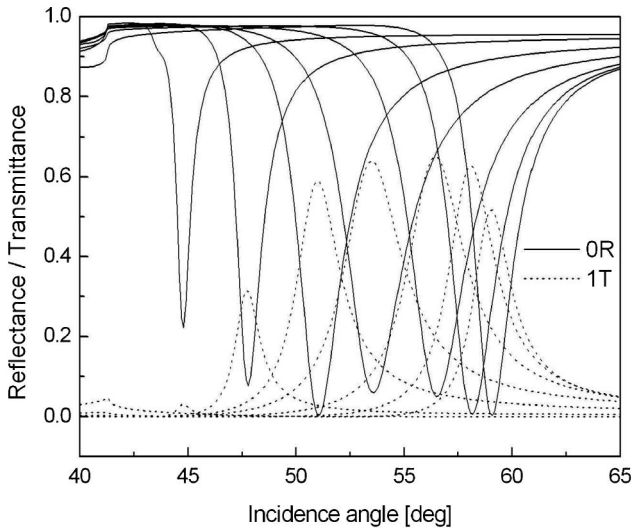

Fig. 3. Calculated reflectance (0R, the solid line) and transmittance curves (1T, the dotted line) for a rectangular grating as a function of incidence angle when d_g varies from 30 nm to 300 nm.

resonance angle displays a gentle increment because the change in d_g causes the local refractive index surrounding the metal film to effectively increase. However, the slope is not constant due to the intrinsic nonlinearity of the dispersion relation of the excited SPs at resonance. The transmittance rapidly increases to 60% until d_g reaches 100 nm, and a high transmittance over 60% is maintained when the thickness is 100–250 nm [see Fig. 4(b)]. No further increase of transmittance at $d_g > 100$ nm can be explained by a limited penetration depth of SP waves with rapidly decaying intensity when one moves further away from the metal surface. For $d_g >$ 250 nm, a reduction in transmittance appears since other diffraction orders become more pronounced. Therefore, for a rectangular grating, the optimal thickness with maximum efficiency was determined to be $d_g = 180$ nm with $1T_{MAX} = 65.3\%$.

In Fig. 3, it is also noteworthy that the minimum reflectance at resonance (MRR) is influenced by the grating thickness. Here, the MRR indicates an intensity of incident beam converted into SPs, and thus a deeper MRR would be desired for a larger excitation of SP waves and a stronger diffracted light. Figure 5(a) presents the reflectance characteristics of a rectangular grating on a 40 nm silver film. In the range of $d_g < 50$ nm, a shallow MRR may disturb an effective outcoupling of SP waves. On the other hand, when the grating thickness exceeds 50 nm, more than 90% of incident beam is absorbed, and its energy is mostly used to generate SP waves. As a result, plasmon waves can be highly excited and strongly coupled with dielectric gratings.

In addition to the transmittance, conversion efficiency (CE) is introduced to compare the overall

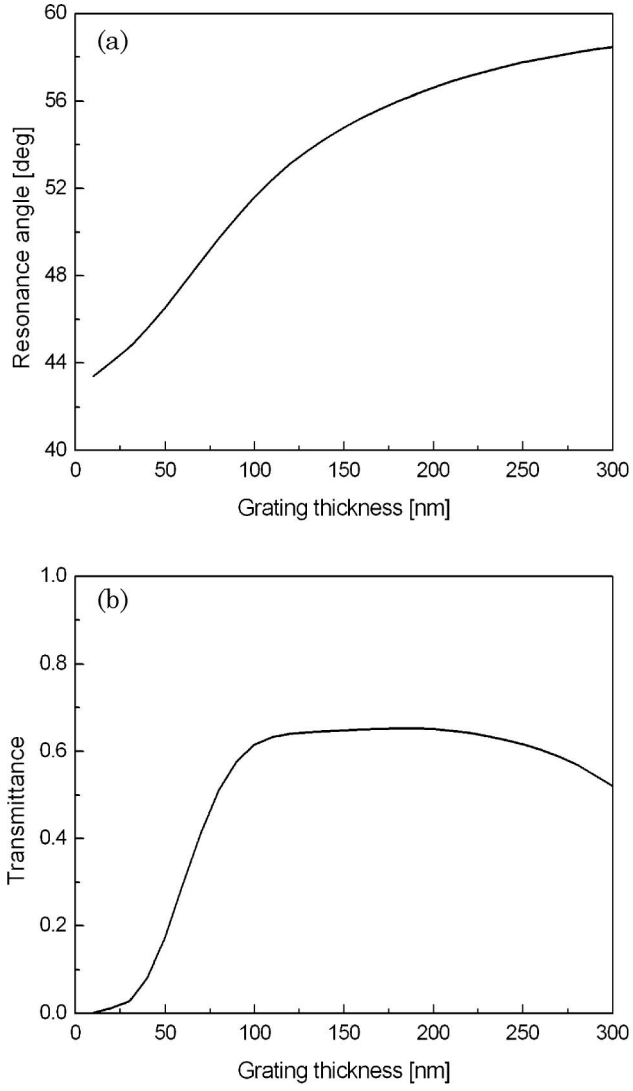

Fig. 4. (a) Resonance and (b) transmittance characteristics of a SPR structure with the rectangular grating. The effects of grating thickness on the resonance angles and transmittance (1T) are shown when grating thickness is increased from 30 to 300 nm in steps of 10 nm. The dielectric grating has a period of $\Lambda = 600$ nm.

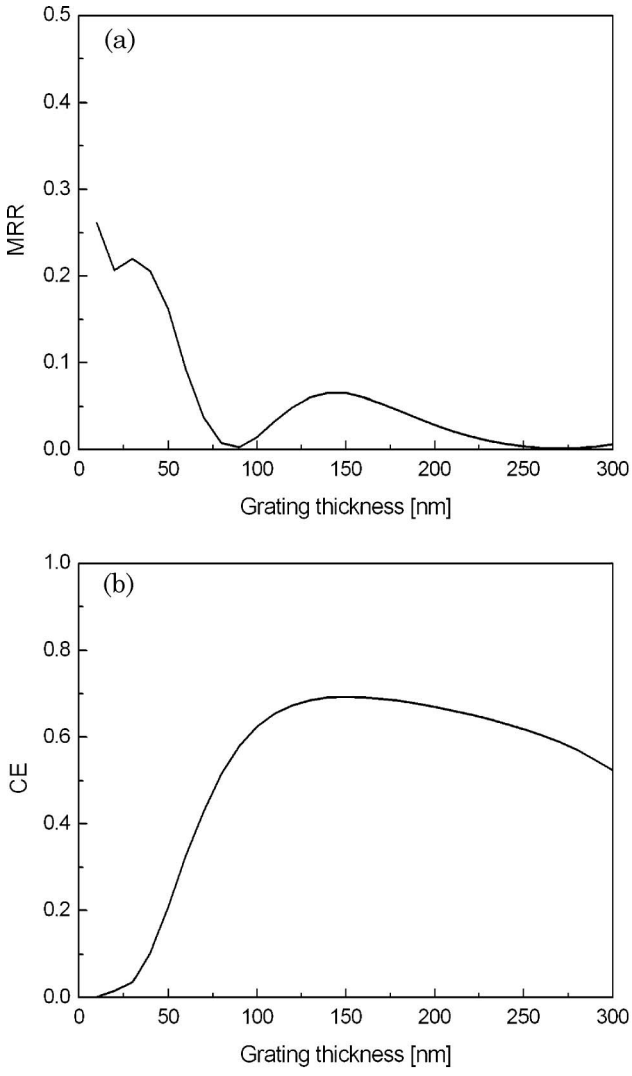

Fig. 5. (a) Minimum reflectance at resonance and (b) conversion efficiency of a SPR structure with rectangular gratings when the grating thickness varies from 30 to 300 nm. The dielectric grating has a period of $\Lambda = 600$ nm.

performance of the SPR structure with dielectric gratings as CE = transmittance/(1 – reflectance) [19]. As the transmitted light is generated by a diffraction of propagating SP waves, the CE is defined as the ratio of the beam energy of the first-order diffraction to the absorbed incidence beam energy into SP waves.

Although a grating-mediated transmission-type SPR structure is required to have a larger CE value approximately equal to 1, we may have difficulties in obtaining such a high CE due to several plasmon damping effects [4]. In Fig. 5(b), the peak CE value for a rectangular grating was determined to be 69.3% at $d_g = 150\,\text{nm}$.

To find the optimal grating structure with the highest diffraction efficiency, we considered various grating profiles, as shown in Fig. 2(b). First, the transmittance characteristics are explored as a function of the grating thickness. Numerical results of four different grating profiles are presented in Fig. 6. After a procedure identical to the one used for the rectangular gratings presented above, the optimal grating thickness was determined to be $d_g = 170\,\text{nm}$ with $1\text{T}_{\text{MAX}} = 68.9\%$ for the pyramid, $d_g = 180\,\text{nm}$ with $1\text{T}_{\text{MAX}} = 62.1\%$ for the left-biased sawtooth, and $d_g = 160\,\text{nm}$ with $1\text{T}_{\text{MAX}} = 58.0\%$ for the right-biased sawtooth. Note that rectangular and pyramid grating profiles have more improved diffraction efficiency than sawtooth profiles. Especially, the pyramid grating presents the highest transmittance among them.

Interestingly, qualitative trends inferred from Fig. 6 agree consistently with the previous works by Moharam and Gaylord [14]. They demonstrated that, when an incident light is diffracted by a dielectric surface relief grating, dielectric gratings with profiles expressed as even functions can provide a larger first-order diffraction efficiency. Thus, if the grating has even symmetry (e.g., pyramid and rectangle profiles in this study), high diffraction efficiencies are possible. However, for grating profiles that lack even symmetry, such as sawtooth profiles, the maximum efficiencies are correspondingly less. This is because the lack of even symmetry produces dephasing of the fundamental first-order diffracted beam and prevents the diffraction efficiency from reaching a large value. In addition, it was demonstrated that higher maximum diffraction efficiencies can be obtained with more pointed grating profiles. This also corresponds well with our results since the pyramid grating, which has a sharper profile than the rectangle grating, shows the highest transmittance. However, it should be emphasized that more dominant factor affecting the maximum diffraction efficiency is the degree of even symmetry in the grating profile.

Second, the CE can be used to estimate the performance of a transmission-type SPR configuration. Similar to the case of the transmittance, pyramid and rectangular gratings showed a greater CE. The peak CE was found at a pyramid profile as presented in Fig. 7. Maximum CE value of each grating profile was obtained to be 70.0% at $d_g = 160\,\text{nm}$ for the pyramid, 62.9% at $d_g = 180\,\text{nm}$ for the left-biased sawtooth, and 58.9% at $d_g = 150\,\text{nm}$ for the right-biased sawtooth profile. In most cases, higher transmittance at the grating profile with even symmetry appears to be attributed to better CE of SP waves. Moreover, while the effect of a sharper grating on the CE is not as high as that on the transmission characteristics, the overall trends are consistent with the results shown in Fig. 6. When taking both the transmittance and CE into consideration, the optimized grating is determined as a pyramid profile. At $\Lambda = 600\,\text{nm}$, these gratings achieve 1T_{MAX} and CE_{MAX} values of about 70%.

For further optimization, the first-order diffraction efficiency of a pyramid profile as a function of grating thickness ($150\,\text{nm} \le d_g \le 400\,\text{nm}$) and period ($200\,\text{nm} \le \Lambda \le 600\,\text{nm}$) was determined [see Fig. 8(a)]. The peak efficiency is 77.1% at $d_g = 310\,\text{nm}$ and $\Lambda = 330\,\text{nm}$. A high transmittance more than 70% is observed over a wide band Δd_g of the grating thickness when the period is 300–400 nm. This Δd_g can measure performance reliability and robustness to fabrication errors in implementing a grating structure and thus, a wide range is desired.

Note, especially, that a significant reduction of diffraction efficiency is found at the period of $\Lambda =$ 450–500 nm and Λ smaller than 300 nm. A possible explanation for this is the effect of radiation damping, which indicates that the incident light is interfered by the diffracted beams [4]. When the grating vector $K\ (= 2\pi/\Lambda)$ is equal to the wave vector k_{SPR} of the SP, backward diffractions of 1R and 2R are generated as shown in Fig. 9(a). This condition can be expressed as

$$K = k_{\text{SPR}} = k_0\sqrt{\varepsilon_p}\sin\theta_{\text{SPR}} = \frac{2\pi}{\Lambda}. \tag{5}$$

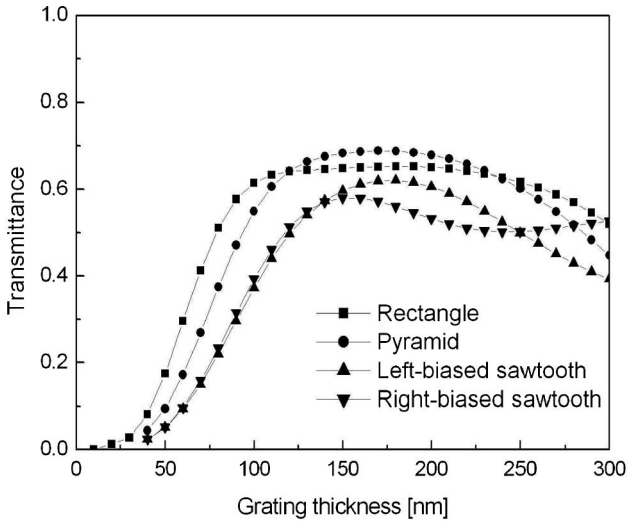

Fig. 6. Transmittance characteristics of four different grating profiles as a function of the grating thickness.

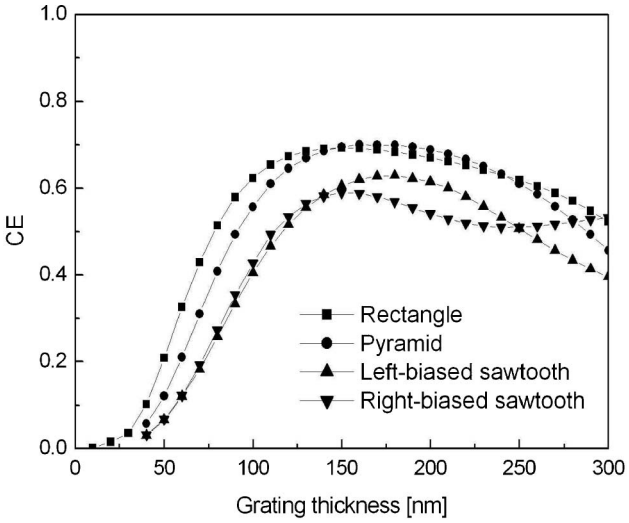

Fig. 7. Conversion efficiencies of four different grating profiles as a function of the grating thickness.

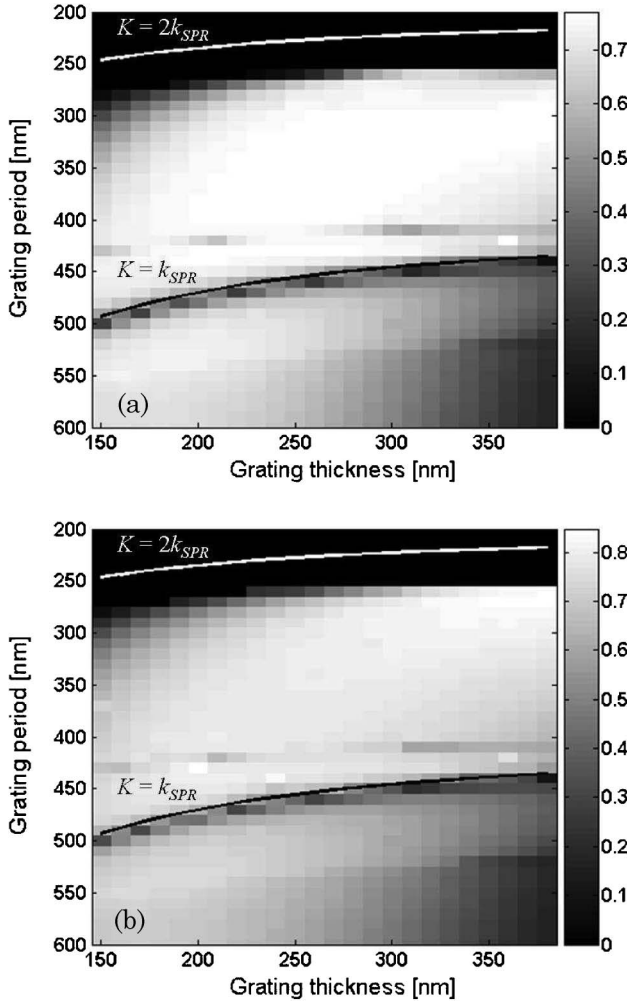

Fig. 8. (a) Transmittance and (b) conversion efficiency of the first-order diffraction beam for the pyramid grating when the grating thickness varies from 150 nm to 400 nm and the period from 200 nm to 600 nm. The black and white lines indicate the resonance conditions of $K = k_{\mathrm{SPR}}$ and $K = 2k_{\mathrm{SPR}}$, respectively.

At this resonance, since the diffracted light of 2R has a reflection angle of θ_{SPR}, its trace overlaps the incidence and a destructive interference may occur. As a result, the excitation of SP waves is fairly disturbed and weak transmittance appears. This is confirmed in Fig. 8, since the line $K = k_{\mathrm{SPR}}$ obtained from Eq. 5 matches well with the dark region, which has a low transmittance.

Additionally, at the resonance condition that satisfies $K = 2k_{\mathrm{SPR}}$, only one backward diffraction order (1R) is generated, and it propagates with an angle of θ_{SPR}, which can be described by

$$K = 2k_{\mathrm{SPR}} = 2k_0\sqrt{\varepsilon_p}\sin\theta_{\mathrm{SPR}} = \frac{2\pi}{\Lambda}. \qquad (6)$$

Figure 9(b) shows that the incident beam can be highly degenerated through a severe destructive coupling between the incidence and the diffracted light. The reduction of transmitted intensity might be more considerable because the backward diffraction of 1R is strong enough to be comparable to the incidence. Thus, transmittance around the line $K = 2k_{\mathrm{SPR}}$ is found to be negligible as shown in Fig. 8(a). In the case of the CE, the distributions are similar to those of the transmittance as shown in Fig. 8(b). $\mathrm{CE_{MAX}} = 84.7\%$ was obtained at $d_g = 200$ nm and $\Lambda = 430$ nm.

As an application example of the SPR configuration discussed in this study, an optimal dielectric grating with pyramid profile at $d_g = 310$ nm and $\Lambda = 330$ nm on a silver film is now applied as an optical biosensor. To quantify the sensitivity with respect to changes in refractive index of the dielectric media surrounding sensor surfaces, target binding between biomolecules is modeled as 3 nm thick dielectric monolayer. Figure 10 shows that, for a conventional reflection-type, incidence angle with minimum reflectance (0R) shifts from 43.13° to 43.26° as the refractive index of binding layer varies from 1.40 to 1.80 in steps of 0.05. On the other hand, the incidence angle with maximum transmittance (1T) of a transmission-type SPR biosensor with a pyramid grating is increased from 71.04° to 71.69°, indicating 5 times better sensitivity. A plasmonic interpretation based on a surface-limited increase of sensing area and an enhanced excitation of local field amplitude at the sharp corners of a pyramid grating can be adopted to explain the sensitivity improvement [20] Linear regression analyses indicate that the shift is highly linear over the whole range of refractive indices. R is the correlation coefficient that denotes the linearity obtainable in the sensor performance, and R values for reflection- and transmission-type SPR configurations are 0.99625 and 0.99745, respectively.

Finally, as silver is known to be highly susceptible to oxidation, an interesting possibility is to employ an oxide layer between diffraction gratings and a silver film in order to estimate its effect on transmission characteristics. Although details will be addressed in a subsequent study involving a bimetallic

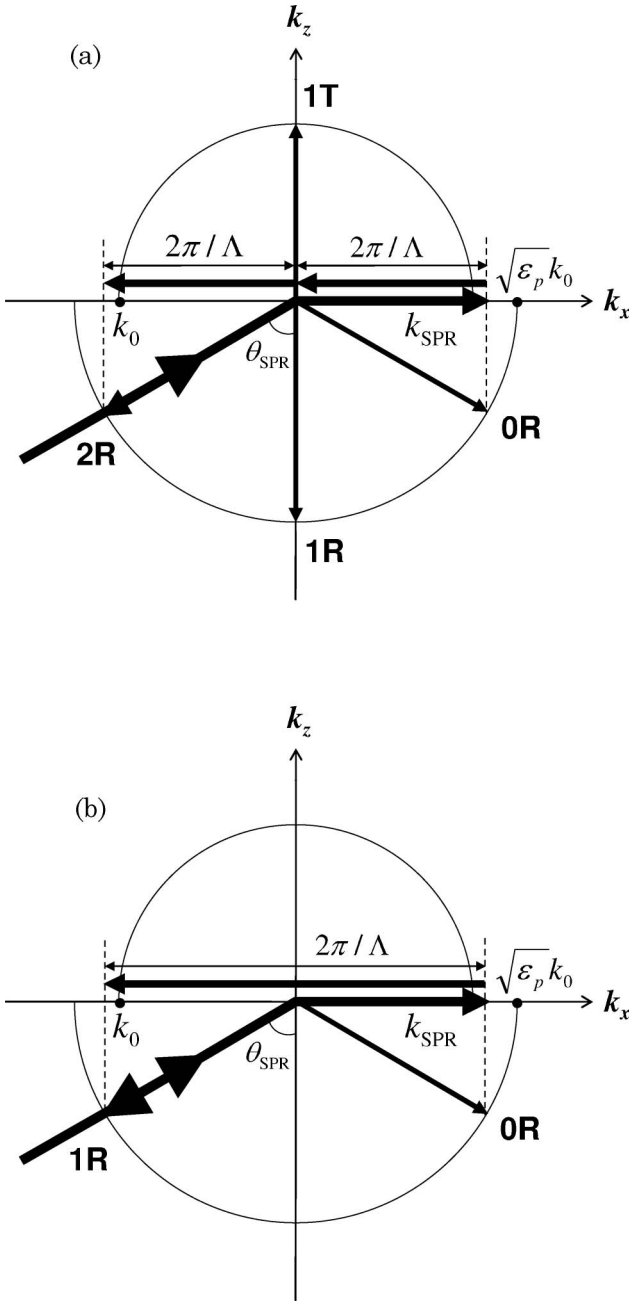

Fig. 9. Phase diagrams of momentum matching between the SP and photon when (a) $K = k_{SPR}$ and (b) $K = 2k_{SPR}$.

Au/Ag surface where a thin gold film is added to protect a silver layer from oxidation, the presence of an oxide layer may affect the resonance condition and interaction between dielectric gratings and resonant SP waves.

In view of the large-area and high-throughput production of an SPR structure with dielectric gratings on a metal film, one may take advantage of molding based on nanoimprint lithography. The processes used to fabricate nanograting molds have been developed rapidly [21]. For example, a rectangle grating mold can be fabricated by plasma etching following electron-beam lithography or interference lithography. A pyramid profile can be obtained from a process

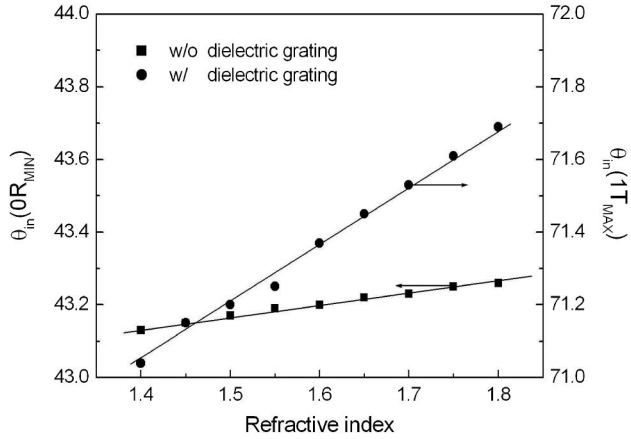

Fig. 10. Linear regression analyses between incidence angle and refractive index of a dielectric binding layer for an SPR biosensor with and without a dielectric pyramid grating of $d_g = 310$ nm and $\Lambda = 330$ nm in an air environment. $\theta_{in}(0R_{MIN})$ and $\theta_{in}(1T_{MAX})$ denote the incidence angle at minimum reflectance and maximum transmittance, respectively.

combining interference lithography and anisotropic wet chemical etching [22]. For sawtooth profiles, a process of directional interference lithography followed by ion etching or of patterning on off-cut wafers with interference lithography followed by anisotropic etching can be utilized [23]. Although controlling geometric parameters of pyramid and sawtooth nanograting molds with precision to achieve uniform patterns in a reproducible manner remains a challenge compared to working with a rectangle profile, the relevant fabrication work is currently under way.

This study suggests the need for considering the grating parameters and their effects on the transmittance, since the transmittance achieved in a grating-based SPR structure can be compromised depending on the grating design. The diffracted light from the SP waves can be applied to active or passive optical devices, such as optical imaging systems, polarization filters, and optical modulators.

4. Concluding Remarks

In this study, we examined the impact of grating parameters on the transmittance of a grating-mediated SPR structure using RCWA. Dielectric gratings built on a silver film led to a significant diffraction efficiency of propagating SP waves and gratings with a pyramid profile had a higher transmittance than the other profiles. The effect of grating profile on the transmission efficiency was discussed using the degree of symmetry and sharpness.

In addition, optimal parameters of the dielectric gratings were determined based on quantitative measure of the first-order diffraction efficiency and the CE. Optimal gratings were found to be the pyramid profiles with maximum transmittance of 77.1% at $d_g = 310$ nm and $\Lambda = 330$ nm and maximal CE value of 84.7% at $d_g = 200$ nm and $\Lambda = 430$ nm. Moreover, there was a relatively large width of grating thickness Δd_g (more than 100 nm), in which the

transmittance exceeds 70% when the period ranges 300–400 nm, indicating that this design would be robust against fabrication errors. An abrupt decrease in transmittance was also clarified based on the effects of radiative damping. Our study on a grating-mediated transmission-type SPR configuration demonstrates the possibility of transmission improvement and the potential of using transmitted SP waves in various optical devices.

This research was supported by the Kyung Hee University Research Fund in 2008 (KHU-20080693).

References

1. T. Okamoto, T. Kamiyama, and I. Yamaguchi, "All-optical spatial light modulator with surface plasmon resonance," Opt. Lett. **18**, 1570–1572 (1993).
2. S. A. Maier and H. A. Atwater, "Plasmonics: localization and guiding of electromagnetic energy in metal/dielectric structures," J. Appl. Phys. **98**, 011101 (2005).
3. J. Homola, S. S. Yee, and G. Gauglitz, "Surface plasmon resonance sensors: review," Sens. Actuators B **54**, 3–15 (1999).
4. H. Raether, *Surface Plasmons on Smooth and Rough Surfaces and on Gratings,* Springer Tracts in Modern Physics (Springer-Verlag, 1988).
5. E. Ozbay, "Plasmonics: merging photonics and electronics at nanoscale dimensions," Science **311**, 189–193 (2006).
6. B. Huang, F. Yu, and R. N. Zare, "Surface plasmon resonance imaging using a high numerical aperture microscope objective," Anal. Chem. **79**, 2979–2983 (2007).
7. J. M. Montgomery and S. K. Gray, "Enhancing surface plasmon polariton propagation lengths via coupling to asymmetric waveguide structures," Phys. Rev. B **77**, 125407 (2008).
8. W. Rothballer, "The influence of surface plasma oscillations on the diffraction orders of sinusoidal surface gratings," Opt. Commun. **20**, 429–433 (1977).
9. M. J. Jory, P. S. Vukusic, and J. R. Sambles, "Development of a prototype gas sensor using surface plasmon resonance on gratings," Sens. Actuators B **17**, 203–209 (1994).
10. S. Park, G. Lee, S. H. Song, C. H. Oh, and P. S. Kim, "Resonant coupling of surface plasmons to radiation modes by use of dielectric gratings," Opt. Lett. **28**, 1870–1872 (2003).
11. C. Lenaerts, F. Michel, B. Tilkens, Y. Lion, and Y. Renotte, "High transmission efficiency for surface plasmon resonance by use of a dielectric grating," Appl. Opt. **44**, 6017–6022 (2005).
12. K. M. Byun, S. J. Kim, and D. Kim, "Grating-coupled transmission-type surface plasmon resonance sensors based on dielectric and metallic gratings," Appl. Opt. **46**, 5703–5708 (2007).
13. M. C. Hutley, *Diffraction Gratings* (Academic, 1982).
14. M. G. Moharam and T. K. Gaylord, "Diffraction analysis of dielectric surface-relief gratings," J. Opt. Soc. Am. **72**, 1385–1392 (1982).
15. L. Li and C. W. Haggans, "Convergence of the coupled-wave method for metallic lamellar diffraction gratings," J. Opt. Soc. Am. A **10**, 1184–1189 (1993).
16. Y.-J. Hung, I. I. Smolyaninov, Q. Balzano, and C. C. Davis, "Strong optical coupling effects through a continuous metal film with a surface dielectric grating," Proc. SPIE **5927**, 386–394 (2005).
17. K. M. Byun, S. J. Kim, and D. Kim, "Design study of highly sensitive nanowire-enhanced surface plasmon resonance biosensors using rigorous coupled wave analysis," Opt. Express **13**, 3737–3742 (2005).
18. K. M. Byun, S. J. Yoon, D. Kim, and S. J. Kim, "Experimental study of sensitivity enhancement in surface plasmon resonance biosensors by use of periodic metallic nanowires," Opt. Lett. **32**, 1902–1904 (2007).
19. S. Park, H. S. Won, G. Lee, S. H. Song, C. H. Oh, and P. S. Kim, "Grating-assisted emission of surface plasmons," J. Korean Phys. Soc. **46**, 492–497 (2005).
20. K. M. Byun, D. Kim, and S. J. Kim, "Investigation of the profile effect on the sensitivity enhancement of nanowire-mediated localized surface plasmon resonance biosensors," Sens. Actuators B **117**, 401–407 (2006).
21. J. A. Rogers and R. G. Nuzzo, "Recent progresses in soft lithography," Mater. Today **8**, 50–56 (2005).
22. Z. Yu and S. Y. Chou, "Triangular profile imprint molds in nanograting fabrication," Nano Lett. **4**, 341–344 (2004).
23. C.-H. Chang, R. K. Heilmann, R. C. Fleming, J. Carter, E. Murphy, M. L. Schattenburg, T. C. Bailey, J. G. Ekerdt, R. D. Frankel, and R. Voisin, "Fabrication of sawtooth diffraction gratings using nanoimprint lithography," J. Vac. Sci. Technol. B **21**, 2755–2759 (2003).